Published in final edited form as:
J Biol Chem. 2007 March 23; 282(12): 8837–8847.

The Function of Guanylate Cyclase 1 and Guanylate Cyclase 2 in Rod and Cone Photoreceptors*,S

Wolfgang Baehr‡,§,¶,1, **Sukanya Karan**‡,§, **Tadao Maeda**‖, **Dong-Gen Luo****, **Sha Li**‡, **J. Darin Bronson**‡, **Carl B. Watt**‡, **King-Wai Yau****, **Jeanne M. Frederick**‡, and **Krzysztof Palczewski**‖

‡*Department of Ophthalmology and Visual Sciences, University of Utah, Salt Lake City, Utah 84112*

§*Department of Biology, University of Utah, Salt Lake City, Utah 84112*

¶*Department of Neurobiology and Anatomy, University of Utah, Salt Lake City, Utah 84112*

‖*Department of Pharmacology, Case Western Reserve University, Cleveland, Ohio 44106*

***Department of Neuroscience, Johns Hopkins University School of Medicine, Baltimore, Maryland 21205*

Abstract

Retinal guanylate cyclases 1 and 2 (GC1 and GC2) are responsible for synthesis of cyclic GMP in rods and cones, but their individual contributions to phototransduction are unknown. We report here that the deletion of both GC1 and GC2 rendered rod and cone photoreceptors nonfunctional and unstable. In the rod outer segments of GC double knock-out mice, guanylate cyclase-activating proteins 1 and 2, and cyclic GMP phosphodiesterase were undetectable, although rhodopsin and transducin α-subunit were mostly unaffected. Outer segment membranes of GC1$^{-/-}$ and GC double knock-out cones were destabilized and devoid of cone transducin (α- and γ-subunits), cone phosphodiesterase, and G protein-coupled receptor kinase 1, whereas cone pigments were present at reduced levels. Real time reverse transcription-PCR analyses demonstrated normal RNA transcript levels for the down-regulated proteins, indicating that down-regulation is posttranslational. We interpret these results to demonstrate an intrinsic requirement of GCs for stability and/or transport of a set of membrane-associated phototransduction proteins.

The second messenger for phototransduction in rods and cones of the vertebrate retina, cyclic GMP (cGMP),[2] is presumed to be synthesized by guanylate cyclases GC1 (1) (GC-E) and GC2 (GC-F) and particulate enzymes and integral membrane proteins with a single transmembrane domain (1-3). GC1 is detected in the retina, pineal gland, and olfactory bulb (4) as well as the cochlear nerve and the organ of Corti (5), whereas GC2 is found only in the retina. The activities of these enzymes are Ca^{2+}-sensitive, a sensitivity that is mediated by guanylate cyclase-activating proteins (GCAPs). GCAPs are Ca^{2+}-binding proteins with three high affinity Ca^{2+}-binding sites (EF hands) (6-8). In light, the activation of cGMP phosphodiesterase (PDE6) in

*This work was supported by National Institutes of Health Grants EY09339 and P30 EY11373 (to K. P.), EY08123 and P30 EY014800 (to W. B.), and EY06837 (to K. W. Y.); a grant from Research to Prevent Blindness, Inc. (to the Departments of Ophthalmology at the University of Utah), and a Center grant of the Foundation Fighting Blindness, Inc. (Owings Mills, MD) (to the University of Utah).

S The on-line version of this article (available at http://www.jbc.org) contains supplemental Table S1 and Figs. S1–S4.

1To whom correspondence should be addressed: Moran Eye Center, University of Utah Health Science Center, 65 N. Medical Dr., Salt Lake City, UT 84132-5330. Tel.: 801-585-6643; Fax: 801-585-1515; E-mail: wbaehr@hsc.utah.edu.

This paper is dedicated to the memory of Kimberly A. Howes (1956 –2007).

2The abbreviations used are: cGMP, cyclic GMP; COS, cone outer segments; ERG, electroretinogram; GC, guanylate cyclase; GC1, guanylate cyclase 1 (synonymous with GC-E); GC2, guanylate cyclase 2 (synonymous with GC-F); GCAP, GC-activating protein; GCdko, GC double knock-out; GRK1, G protein-coupled receptor kinase 1; LCA, Leber congenital amaurosis; PDE6, photoreceptor cGMP phosphodiesterase 6; PDE6α′, cone PDE6 α subunit; ROS, rod outer segments; WT, wild type; pAb, polyclonal antibody; mAb, monoclonal antibody; cd, candela; CNG, cyclic nucleotide-gated; RT, reverse transcription.

rods and cones leads to the hydrolysis of cGMP and the closure of cGMP-gated (CNG) cation channels (for a review, see Ref. 9). Channel closure causes the cytosolic free Ca^{2+} concentration to decline. The resulting dissociation of Ca^{2+} from the GCAPs increases the activity of the GCs and therefore the cGMP level, completing the negative feedback loop (10). Thus, GCs are not only important for maintaining the basal cGMP level in darkness but are also critical for expediting the recovery of photoreceptors following light stimulation. Of the two GCAPs present in mouse retina, GCAP1 stimulates GC1 more efficiently than GC2 (11). Deletion of both GCAP genes delays recovery of the dark current due to loss of Ca^{2+}-dependent GC activation (12).

In addition to particulate GCs, a role in photoreceptor physiology was envisioned for soluble GCs, but no genetic or functional evidence is available for a role in modulation of cGMP in photoreceptors (13,14). In humans, null mutations in the GC1 gene (*GUCY2D*, on chromosome 17) are known to cause Leber congenital amaurosis type 1 (LCA1), an autosomal recessive, early onset rod/cone dystrophy (15,16). A naturally occurring retinal degeneration in chicken (*rd* or *GUCY1*B* chicken), caused also by a null mutation in the GC1 gene (17), mimics the human LCA phenotype. In mice, however, a null mutation in the GC1 gene produces a cone dystrophy; the $GC1^{-/-}$ rods remain viable and responsive to light (18,19). No human retinal disease has yet been linked to a defect in the GC2 gene (*GUCY2F*, on the X chromosome). Here, the functional role of GC2 was examined by deleting the mouse GC2 gene. Our results show that electroretinographic (ERG) responses are largely normal in $GC2^{-/-}$ retina. In contrast, the ERG responses of GC1/GC2 double knock-out (GCdko) mice are absent, suggesting that no GC other than GC1 and GC2 is involved in rod or cone phototransduction. Histology of GCdko retinas revealed that outer segments form but degenerate in a manner similar to that observed in the *rd* (*GUCY1*B*) chicken (17) and in human LCA1 patients (20). Ultrastructural analyses detailed abnormal outer segment morphologies. Down-regulation of PDE6 and GCAPs in GCdko rods as well as down-regulation of cone phototransduction components in $GC1^{-/-}$ cones suggest that GCs serve enzymatic, stabilizing, and structural/transport roles in photoreceptors.

MATERIALS AND METHODS

Construction of Targeting Vector and Generation of GC2 Knock-out Mice

To delete the GC2 gene, a 16-kb mouse genomic DNA fragment containing exon 1 was cloned from a mouse 129Sv/Ev λ genomic library. An 8.5-kb XbaI fragment was subcloned to produce the targeting vector. One side of the *neo* gene cassette was inserted 5 bp upstream of the ATG start codon in exon 2. The replaced sequence starts with 5′-AGGCT**ATG**TTCCTCGGACCCTGGCCTTTTTCTCGCC. The other side of the *neo* gene cassette was inserted 290 bp downstream of the ATG start codon inside exon 2, and that replaced sequence reads 5′-ATTCGAAGGAGTAACTCCTGTCAAATGTCTTGTCCCGG. In this strategy, the *neo* cassette replaced part of the coding region of exon 2. Ten micrograms of the targeting vector were linearized by NotI and then transfected by electroporation of iTL1 ES cells (129Sv/Ev) embryonic stem cells. After selection in G418, surviving colonies were expanded; PCR analysis was performed using primer pair Gctoda6 and PLA2 to identify recombinant clones. Primer Gctoda6 is located 165 bp downstream of the XbaI site, on the short arm side, with a sequence of 5′-GTTCTGAGCTACAGATCCTACAGTG. Primer PLA2 is located in the 5′-promoter region of the *neo* gene cassette and has a sequence of 5′-GTTCTTCGGACGCCTCGTCAACAC. The positive clones gave rise to a 1.5-kb PCR fragment. Correctly targeted ES cell lines were microinjected into C57BL/6J blastocysts. Chimeric mice were generated and gave germ line transmission of the GC2 knock-out to progeny. Primer pair Gctoda6 and Gctowt1 was used to identify the WT allele by its 1.3-kb amplified product. Primer Gctowt1 is located 280 bp downstream of the ATG start codon inside

exon 1, inside the *neo* cassette replaced area, with a sequence of 5′-CAAGACATTTGACAGGAGTTACTC. Alternatively, primer Gctowt1 can be exchanged for primer Gctowt2, which is located 6 bp upstream of primer Gctowt1, with a sequence of 5′-CTGCTTTAGCAATTGAGCGAATCAG. Amplification yields a 1.3-kb fragment. PCR conditions were 94 °C for 20 s, 62 °C for 60 s, and 72 °C for 120 s (35 cycles). In difficult amplifications, 10% Me_2SO or Q solution from Qiagen was used.

GC1$^{-/-}$ and Double Knock-out Mice

Procedures for the animal experiments described here were IACUC-approved by the University of Utah and Case Western Reserve University and conformed to recommendations of the Association of Research for Vision and Ophthalmology. Animals were maintained in complete darkness, or cyclic light (12 h light/12 h dark or 14 h light/10 h dark) conditions, and physiological experiments were performed under dim red illumination using a Kodak number 1 Safelight filter (transmittance >560 nm). GC1 knock-out mice were rederived from GC1 knock-outs (19) using mice originally produced by Dr. David Garbers (University of Texas Southwestern, Dallas, TX) (18). GC single and double knock-outs were typed for the presence of GC1 and GC2 knock-out alleles and absence of WT alleles. Primers used for GC1 genotyping were as follows: Gc1F4 (forward primer in intron 4), 5′-TCCTATCCACGACAGGACCAAGACTGT; Gc1R4 (reverse primer in intron 5), 5′-GAGAGCAGAAGGGTAGCATTAGCTCAG; NeoF4 (forward primer in *neo* cassette), 5′-ACCGCTATCAGGACATAGCGTTGGCTA. Both pairs of primers were used in a one-tube PCR amplification to yield the fragments shown in Fig. 1*D*. GC2$^{-/-}$ mice were genotyped using forward primer Pla2 and reverse primer Gc2mt-R2 (5′-GTGCCTACAGGACTCTTGATGTCATTC). WT mice were genotyped with primers Gctowt1 and Gctoda6.

Antibodies

The following laboratories have generously provided antibodies: David Garbers, University of Texas Southwestern (pAb L670, anti-GC2), Tiansen Li, Harvard University (anti-PDE6α'), Cheryl Craft, University of Southern California (anti-cone arrestin, mCAR or LUMIJ), Ching-Kang Chen, Virginia Commonwealth University (UUTA, anti-rod transducin α subunit), Robert Molday, University of British Columbia (1D4, anti-rhodopsin, and anti-CNGA1 subunit antibody), and Rick Cote, University of New Hampshire (anti-PrBP/δ (PDEδ-FL). The following antibodies were commercially available: anti-cone Tγ and anti-PDE6 (MOE, Cytosignal Research Products), anti-cone Tα (Santa Cruz Biotechnology, Inc., Santa Cruz, CA); anti-S opsin and anti-M/L opsin (Chemicon/Millipore, Temecula, CA).

Real Time RT-PCR

Semiquantitative real time RT-PCR was performed using total RNA of WT and GCdko retinas. The following primers were used: rod PDE6α subunit forward, 5′-TGATGAGTACGAAGCCAAGATGAAGGC; rod PDE6α subunit reverse, 5′-TCAGCTACTGGATGCAACAGGACTTAG; rod Tα subunit forward, 5′-ACGCTGTCACCGACATTATCATCAAGG; rod Tα subunit reverse, 5′-AGCAGCTTGTGGAAAGGACGGTATTTG; cone Tα subunit forward, 5′-ATGACCTGTGCTACAGACACACAGAAC; cone Tα subunit reverse, 5′-GCATGAAGCCTCAGATTCTAAGCTTGC; GCAP1 forward, 5′-AGTTGCGCTGGTATTTCAAGCTCTACG; GCAP1 reverse, 5′-AAACACGGTATCTGTGAATTCCTCGGC; GCAP2 forward, 5′-TATGTAGAGAGCATGTTCCGAGCCTTC; GCAP2 reverse, 5′-ATGCAGCCATTTCGGTCCTTGTCATAG; Gapdh forward, 5′-acccctttcattgacctcaactacatgg; Gapdh reverse, 5′-atttgatgttagtggggtctcgctccT. All primer pairs

were designed to give an amplicon size of ~150 bp. Total RNAs were extracted from 1-month-old mouse retina by using Trizol reagent (Invitrogen) followed by DNase digestion. Real-time RT-PCR was performed with both WT and GCdko RNA samples (25 ng) using the QuantiTect SYBR green RT-PCR kit (Qia-gen Inc., Valencia, CA) and a DNA Engine Opticon 2 system (MJ Research, Waltham, MA). Standard curves for each primer set were obtained with 0, 10, 20, 40, 80, and 160 ng of the WT RNA sample (Fig. S3). Results were normalized to Gapdh signals for each sample. Standards for Gapdh and all other primer sets showed similar slopes, indicating equivalent amplification kinetics (Fig. S3).

Confocal Immunolocalization

Eyes were harvested at mid-morning under ambient illumination (200–800 lux) without dark or light adaptation. Left eyes of age-matched mice were immersion-fixed for 2 h using freshly prepared 4% paraformaldehyde in 0.1 M phosphate buffer (pH 7.4) and cryoprotected. Immunocytochemistry was performed as described (21). Affinity-purified primary antibodies (15–25 μl) were applied to each group of four sections in a humidified, rotating chamber overnight at 4 °C. Propidium iodide (Invitrogen Molecular Probes ™; 1:3,000 dilution) was added to the solution containing fluorescein isothiocyanate-conjugated secondary antibody. The sections were viewed using a Zeiss LSM 510 inverted Laser Scan confocal microscope with a ×40, 1.3 numerical aperture oil objective lens and optical slit setting of <0.9 μm. The following antibodies and dilutions were used: anti-GC1 (mAb 1S4, 1:1,000) (22); anti-GC2 (L-670, 1:2000); anti-GCAP1 (pAb UW14, 1:1,000) (23); anti-GCAP2 (pAb UW50, 1:4,000) (24); anti-rhodopsin (mAb 1D4, 1:1,000); anti-rod Tα (UUTA, 1:1,000); anti-rod PDE6 (MOE, 1:1,000); anti-S opsin (1:500); anti-M/L opsin (1:500); anti-cone arrestin (mCAR, 1:1,000); anti-cone PDE6α' (1:4,000); anti-cone Tα (1:500); anti-cone Tγ (1:500); anti-GRK1 (G8, 1:800) (25).

Immunoblotting

Retinas from both eyes of the mouse were sonicated in 100 μl of lysis buffer (26). Each sample (15 μg of protein) was separated on a 10–12% SDS-PAGE, transferred onto a polyvinylidene difluoride filter, and probed with primary antibodies followed by horseradish peroxidase-conjugated secondary antibody. The signal was visualized using chemiluminescence (ECL Plus system (Amersham Biosciences).

ERGs

The recording procedure was performed as described (27,28). ERGs were recorded with the universal testing and electrophysiologic system UTAS E-3000 (LKC Technologies, Inc.). The light intensity was calibrated by the manufacturer and computer-controlled. Flash stimuli had a range of intensities (−3.7-2.8 log cd·s·m^{-2}), and white light flash duration was adjusted according to intensity (from 20 μs to 1 ms). Leading edges of the ERG responses were fitted with a model of rod photoreceptor activation (29). The double-flash recording followed a previously published protocol (30). The normalized amplitude of the probe flash a-wave *versus* the time between two flashes was plotted and fit by the linear regression algorithm in the SigmaPlot program (version 9.0). Dark-adapted ERG recordings after intense constant illumination were performed and evaluated as described (28,31).

Single Cell Recordings

Single cell recordings were performed as described previously (32). An individual rod outer segment was drawn into a snug-fitting glass suction electrode containing 140 mM NaCl, 3.6 mM KCl, 2.4 mM $MgCl_2$, 1.2 mM $CaCl_2$, 3 mM HEPES, pH 7.4, 0.02 mM EDTA, and 10 mM glucose. Membrane current was monitored with a current-to-voltage amplifier (Axopatch 200B, Axon Instruments, CA). All signals were low pass-filtered at 20 Hz (8-pole Bessel) and

sampled at 500 Hz. The light stimulus consisted of brief flashes (10 ms) of unpolarized 500-nm (10-nm bandwidth) light with intervals of 8 s.

Histology

Right eyes of 1–2-month-old WT, GC1$^{-/-}$, GC2$^{-/-}$, and GCdko mice were prepared for light microscope plastic sections and electron microscope thin sections as described (33). For electron microscopy, the eyecups were postfixed in 1% osmium tetroxide in phosphate buffer for 1 h, dehydrated through an ascending series of graded ethanols, and embedded in Spurr's resin. Sections 0.5–1 μm thick and passing through the optic nerve were imaged using a Leica DM-R microscope with Prior stage, using Syncroscan RT software from Syncroscopy. Scaling for measurement was 182 nm/pixel and 5.5 pixels/micrometer at ×40 magnification.

RESULTS

Generation of GC2$^{-/-}$ and GC1/GC2 Double Knock-out (GCdko) Mice

The GC1 (*Gucy2e*, on mouse chromosome 11) and the GC2 (*Gucy2f*, on the X chromosome) genes are closely related in structure (Fig. 1, *A* and *B*) (34). The GC1 knock-out construct (18) replaced a portion of exon 5 encoding the transmembrane domain by a *neo* cassette, thereby deleting the entire intracellular region of GC1. We prepared a GC2 knock-out mouse by replacing a portion of exon 2 containing the translation start codon and the peptide leader sequence with a *neo* cassette (Fig. 1, *B* and *C*). Several generations of these mice were established on the C57BL/6J background and were cross-bred with GC1$^{-/-}$ mice to generate GCdko mice. The GCdko mice were fertile and developed normally, thereby excluding a vital role for GC1 or GC2 during embryogenesis. The genotypes of single and double knock-out mice were confirmed by PCR amplification using GC1- and GC2-specific oligonucleotides (Fig. 1*D*). Immunoblots of GC1$^{-/-}$ and GC2$^{-/-}$ retinal lysates probed with monoclonal anti-GC1 and polyclonal anti-GC2 antibodies confirmed that GC1 and GC2 were not expressed (Fig. 1*E*). Further, immunoblots with anti-GC1 and anti-GC2 antibodies showed that the GC1 expression level is maintained in GC2$^{-/-}$ retina and that the GC2 expression level is also maintained in GC1$^{-/-}$ retina (Fig. 1*F*).

GCdko Rod and Cone Photoreceptors Are Physiologically "Silent"

To test for photoreceptor function in WT and single and double knock-out retinas, we performed full-field ERGs (Table 1 and Fig. 2). Consistent with a previous report (18), scotopic a- and b-wave amplitudes recorded from 4 – 6-week-old GC1$^{-/-}$ mice were significantly reduced compared with WT responses (Fig. 2, *A* and *B*). However, scotopic ERG responses were absent in GCdko mice at all light intensities tested. These results suggest that the rod responses recorded from GC1$^{-/-}$ retinas reflect GC2 activity. Scotopic ERG responses recorded from GC2$^{-/-}$ mice closely resembled those of WT mice, implying that GC1 alone is able to support rod function under these conditions. The a-wave amplitude and sensitivity of the scotopic GC2$^{-/-}$ mouse photoresponse were similar to WT at low intensities (Fig. 2*B*; Table 1); however, at high intensities, GC2$^{-/-}$ a-wave amplitudes were slightly reduced compared with WT (Fig. 2*B*). Photopic ERG responses recorded in the presence of background light were absent in GC1$^{-/-}$ and GCdko mice, whereas GC2$^{-/-}$ a- and b-waves were nearly identical to WT (Fig. 2, *C* and *D*). These results are consistent with GC1 regulating cGMP synthesis in cones and with both GC1 and GC2 regulating cGMP synthesis in rods. Given these observations, the possibility that other cyclases participate in rod or cone phototransduction can be excluded.

Recovery from Test Flashes as Determined by Paired Flash Analysis

A paired flash protocol was used to evaluate the ability of GC deletion mutant retinas to recover responsiveness after light stimulation (23,30,35). In this method, short test flashes followed by varying interstimulus intervals, and a probe flash were used to test for a-wave recovery (36,37). As expected, GCdko photoreceptors were unresponsive (Fig. 3*A*). Recoveries of a-waves measured from $GC1^{-/-}$ mice and $GC2^{-/-}$ mice were normalized to the amplitudes of corresponding WT a-wave responses. Rates of dark current recovery in $GC1^{-/-}$ and $GC2^{-/-}$ mice after the test flash were not significantly different from WT mice ($GC1^{-/-}$, 895.4 ± 112.2 ms; $GC2^{-/-}$, 1018.1 ± 63.1 ms; WT, 893.3 ± 47.8 ms) (Table 1).

Intense Bleach Delays Recovery of $GC1^{-/-}$ and $GC2^{-/-}$ a-wave Amplitudes

In a second approach, dark adaptation rates were determined by exposing animals to a high intensity bleaching light (500 $cd \cdot s \cdot m^{-2}$) for 3 min and then recording a-wave responses elicited by probe flashes delivered intermittently over the course of a 60-min dark adaptation period (Fig. 3*B*). Under these conditions, 70% of rhodopsin was bleached (28). The ratios of the a-wave responses obtained during the for WT, $GC1^{-/-}$, $GC2^{-/-}$, and GCdko mice were plotted as a function of time in darkness. In WT mice, a-wave amplitudes recovered about 70% after 1 h of dark adaptation. The recovery of a-wave amplitudes was significantly delayed in $GC1^{-/-}$ and $GC2^{-/-}$ mice ($p < 0.001$) compared with WT. Following 1 h of dark adaptation, the amplitudes of the a-waves recorded from $GC2^{-/-}$ and $GC1^{-/-}$ mice had recovered to about 30 and 50%, respectively, of their dark-adapted values. These results suggest that GC1 and GC2 contribute distinctly to the recovery of photoreceptors from exposure to intense bleaching light.

Rod Photoreceptor Single Cell Recordings

The mean dark currents of $GC1^{-/-}$ and $GC2^{-/-}$ rod photoreceptors were not significantly different from the WT currents (12 ± 1.2 pA for WT, 12.7 ± 1.3 pA for $GC1^{-/-}$, and 13.8 ± 1.3 pA for $GC2^{-/-}$) (Fig. 4, *A–C*). In contrast, GCdko rods showed no detectable light-sensitive current (Fig. 4*D*). That cyclic nucleotide-gated (CNG) channels are present at similar densities in the rod outer segments (ROS) of WT and GC single knock-out rods argues that $[cGMP]_i$ levels in darkness are similar for WT, $GC1^{-/-}$, and $GC2^{-/-}$ rods, whereas effectively no cGMP is present in GCdko rods. It therefore follows that the basal activity of *either* GC1 or GC2 is sufficient to maintain dark current in rods. Compensatory up-regulation of the other GC when one is missing may account for this observation; however, immunoblot results suggest normal GC2 levels in $GC1^{-/-}$ mice (Fig. 1*F*) (18). Regarding the light response, the kinetics was broadly similar for all three genotypes (Fig. 4, *A–C*). Sensitivity of $GC2^{-/-}$ rods was quite similar to that of WT rods (half-saturating flash intensity of 52.8 ± 4.9 *versus* 48.6 ± 6.3 photons μm^{-2}), but the sensitivity of $GC1^{-/-}$ rods (half-saturating flash intensity of 13.6 ± 2.5 photons μm^{-2}) was about 3.5-fold higher than WT (Fig. 4*E*) (see also Ref. 18).

Down-regulation of GCAP1, GCAP2, and Rod PDE6 in GCdko Photoreceptors

Confocal immunolocalization was used to monitor the subcellular distribution of GCAPs and PDE6 following GC deletion (Fig. 5). As expected, GC1 was not detectable in $GC1^{-/-}$ and GCdko sections (Fig. 5, *B* and *D*), and GC2 was undetectable in $GC2^{-/-}$ and GCdko retinas (Fig. 5, *G* and *H*). GC1 deletion did not appear to affect GC2 expression, and GC2 deletion did not affect GC1 expression, in agreement with immunoblots (Fig. 1*F*). However, GC1 deletion strongly diminished GCAP1 levels in all outer segments (Fig. 5*J*) and GCAP2 levels in rods to a lesser extent (Fig. 5*N*). GC2 deletion had no obvious effect on GCAP1 or GCAP2 expression (Fig. 5, *K* and *O*). In GCdko photoreceptors, low expression levels of GCAP1 and GCAP2 were confined to the cell bodies and myoid regions of photoreceptors (outer nuclear layer; *ONL*), where biosynthesis occurs (Fig. 5, *L* and *P*). Essentially no GCAPs were

detectable in GCdko outer segments that, at this age, showed signs of early degeneration. The immunolabeling patterns of rhodopsin (Fig. S1, *A–D*) and transducin α-subunit (Tα; gene symbol *Gnat1*) (Fig. S1, *E–H*) were mostly normal. However, the labeling patterns of rhodopsin kinase (Fig. 6*T*) and rod transducin α-subunit (Fig. S1*H*) were consistently "patchy" over GCdko ROS.

In GC1$^{-/-}$ and GC2$^{-/-}$ photoreceptors, the immunolabeling patterns of PDE6 subunits (PDE6α, PDE6β, and PDE6γ) (Fig. 5, *R* and *S*) were apparently normal and similar to WT, with highest labeling observed over ROS. However, rod PDE6$\alpha\beta\gamma$ subunits were undetectable in GCdko frozen sections using an antibody (MOE) recognizing all three subunits (Fig. 5*T*). Double labeling with anti-GRK1 antibody revealed that MOE recognized both rod PDE6 and cone PDE6 (results not shown). Thus, absence of immunolabel in Fig. 5*T* suggested that cone PDE6α' was also down-regulated in the GCdko mutant.

GC1$^{-/-}$ and GCdko Cone Outer Segments Are Unstable

Previous studies showed that GC1$^{-/-}$ cone photoreceptors develop and elaborate outer segments but gradually degenerate (18,38). The subcellular distributions of S- and M/L-pigments that reside exclusively in cone outer segments (COS) and the freely diffusible cone arrestin were investigated in the three GC deletion mutants by immunocytochemistry. S-opsin (Fig. 6, *A–D*) and M/L-opsin (Fig. S2), which normally reside in COS, were present at reduced levels in the GC1$^{-/-}$ and GCdko cones and mislocalized. Extracellular particles, intensely immunopositive for cone pigments, were observed adjacent to the retinal pigment epithelium (*arrows* in Fig. 6, *B* and *D*, and Fig. S2*B*; see also Fig. 8*D*). Cone somata were still abundant at 2 months of age in GC1$^{-/-}$ retinas but with highly disorganized COS (Figs. S2, *B* and *F*, and 8, *C* and *E*), and GCdko retinas had a slightly reduced number of cones as judged by labeling with anti-cone arrestin (Fig. S2*H*). Double labeling with anti-cone arrestin and anti-S-pigment antibodies showed that S-pigment was present in GC1$^{-/-}$ outer segments predominantly in extracellular particles (Fig. S2*J*, *arrows*). GC1$^{-/-}$ and GCdko COS are apparently unstable and disintegrating at the age of 2 months.

Cone Transducin, Cone PDE6α′, and GRK1 Are Undetectable in GC1$^{-/-}$ and GCdko Cone Outer Segments

We next tested for the presence of membrane-associated cone phototransduction proteins in GC mutant COS. Specifically, we examined levels of myristoylated cone Tα, farnesylated cone Tγ, geranylgeranylated cone PDE6α', and farnesylated GRK1 in GC1$^{-/-}$, GC2$^{-/-}$, and GCdko retinas (Fig. 6). All four proteins were undetectable in GC1$^{-/-}$(Fig. 6, *F*, *J*, *N*, and *R*) and GCdko COS (Fig. 6, *H*, *L*, *P*, and *T*). Note that GRK1 immunolabeling distinguishes between rods and cones and was comparable with that of WT in GC1$^{-/-}$ and GC2$^{-/-}$ ROS (Fig. 6, *Q–S*) but was undetectable in GC1$^{-/-}$ and GCdko COS (Fig. 6, *R* and *T*). These results show that essential phototransduction proteins cone Tα, cone Tγ, PDE6α', and GRK1 are either absent or below the threshold of detection in GC1$^{-/-}$ COS.

Down-regulation of Membrane-associated Proteins Is Post-translational

By immunocytochemistry, we observed significant down-regulation of GCAPs, cone Tα, cone Tγ, and cone PDE6α' in GC1$^{-/-}$ and GCdko photoreceptor outer segments, whereas GC2 deletion had no effect on protein levels. Immunoblots (Fig. 7*A*) confirmed that protein levels of GCAPs, cone Tα, and cone arrestin were in part drastically reduced in GC1$^{-/-}$ and GCdko retinas. Absence of rod PDE6 in GCdko rods was also confirmed by immunoblotting; rod PDE6 subunits (α, β, and γ) were undetectable in GCdko retina extracts. In contrast, deletion of either GC singly had no effect on rod PDE6 expression. Rhodopsin, rod Tα, and rod CNG channel subunit α subunit (CNGA1) were present at nearly normal levels in all four genotypes.

Down-regulation of GCAPs was shown to be posttranslational in GC1$^{-/-}$ retina (19). We extend that observation to show that other peripherally associated membrane proteins are also down-regulated. To verify that transcription of genes whose products are down-regulated in GCdko retina is normal, we determined the concentrations of mutant mRNAs relative to WT mRNAs by semiquantitative real time RT-PCR (Fig. 7*B*). Real time RT-PCR analyses of GCAP1, GCAP2, rod PDE6*α*, and cone T*α* transcripts confirmed that mRNA levels were essentially identical in both WT and double knockout retinas. A standard curve indicated similar amplification kinetics for each transcript (Fig. S3). Microarray analysis suggested that the transcript levels of the down-regulated genes (and all other phototransduction genes) in GCdko retina were essentially unchanged (results not shown). Thus, genes encoding GCAPs, rod/cone PDE6, and cone transducin are transcribed normally in the GCdko retina, and down-regulation occurs posttranslationally.

GCdko Retinas Degenerate as in Human LCA

At 2 months of age, outer segment lengths are ~50–70% of normal, suggesting that degeneration progresses relatively slowly in GCdko mice (*e.g.* Fig. 5, *D*, *H*, and *L*). We observed that cone degeneration was consistently most severe inferior to the optic nerve (results not shown); the superior midperiphery was consistently the least degenerated as observed by Coleman *et al.* (19). At 6 months of age, the GCdko outer nuclear layer contains only 4–6 rows of nuclei (Fig. S4*B*, *right*), and ROS lengths are severely reduced in superior/inferior and nasal/temporal quadrants (Fig. S4*A*). Cone cell remnants, particularly synaptic pedicles and somata, can be identified by labeling with anti-cone arrestin (Fig. S4*B*, *bottom*), but outer segments are absent. This finding is consistent with a post-mortem study of an 11-year-old LCA patient with a null mutation in the *GUCY2D* gene. The macula and peripheral retina of this patient revealed a substantial number of cones and rods, but both photoreceptor types lacked outer segments (39).

Ultrastructural Examination Reveals Membrane Partitioning in GC1$^{-/-}$ and GCdko Photoreceptors

To provide a structural framework for the interpretation of immunolocalization, companion eyes were plastic-embedded and sectioned for electron microscopy. GC1$^{-/-}$ retinas were selected for the examination of cones, GCdko retinas were selected for analysis of rods, and each of these was compared with the corresponding photoreceptor of an age-matched WT retina. All observations are derived from mouse retina inferior to the optic nerve, a region where electron-dense granules were frequently encountered in distal inner segments of both WT and knock-out cones (see Fig. 8*B*). GC1$^{-/-}$ cones exhibited problems of varying degree; apical inner segments appeared retracted from connecting cilia and surrounded by extracellular “blebs”; at the distal connecting cilia, membrane components appeared to partition into layered stacks or vesicles/tubules, and in severely degenerated cases, these membranes were detached (Figs. 8, *C* and *E*). Adjacent to the retinal pigmented epithelium, particles consisting of an inner collection of vesicles enclosed by layers of dense membrane were often observed (*e.g.* see Fig. 8*D*) and correspond in position to cone opsin-immunoreactive particles of Fig. 6*B*. GCdko rods, too, were surrounded by blebs in the interphotoreceptor matrix. Distal to the connecting cilia, the ROS were shorter and narrower than their WT counterparts and appeared “banded” with alternating regions of dense membrane layers and lumen-containing tubules (Fig. 8, *G* and *H*) suggesting unconventional ROS membrane assembly.

DISCUSSION

Deletion of integral membrane proteins GC1 and GC2, singly and in combination, has permitted the following observations in mouse photoreceptors. First, GC2 can compensate in part for the absence of GC1 in rods. Second, simultaneous ablation of GC1 and GC2 abolishes

rod and cone phototransduction, thereby excluding the possibility that a third GC (soluble or particulate) participates in the regulation of phototransduction. Third, several peripherally membrane-associated phototransduction components (GCAPs, rod and cone PDE6, and cone transducin) are either absent or severely reduced in $GC1^{-/-}$ and GCdko photoreceptor outer segments. Fourth, $GC1^{-/-}$ and GCdko cone outer segment membranes are disorganized at 1–2 months. Fifth, GCdko rod and cone photoreceptors degenerate with a phenotype simulating human LCA1 (for a phenotype summary of GC knock-outs, see Table S1).

Apart from a minor ERG a-wave amplitude reduction, $GC2^{-/-}$ rod photoreceptors recovered more slowly both in double flash experiments (Fig. 3*A*) and after intense 3-min photobleaching (Fig. 3*B*). The mechanism for the delay is unclear, but it may in part be caused by a reduction in GRK1 (Fig. 7*A*) (40,41). In single cell recordings, $GC2^{-/-}$ rods and WT rods displayed nearly identical half-maximal sensitivity. However, return to the dark state in $GC2^{-/-}$ rods expressing was slightly delayed despite a near normal set of GCAPs (Figs. 5 and 7). $GC1^{-/-}$ retinas, in contrast, had severely reduced scotopic a-and b-waves but recovered faster in double flash experiments and from intense bleaching. $GC1^{-/-}$ rods recovered to the dark state nearly as rapidly as WT rods despite severely reduced levels of GCAPs in their outer segments. This is in contrast to previous results (18) in which $GC1^{-/-}$ rods paradoxically recovered faster than WT rods. The reason for this discrepancy is unknown but may in part be due to genetic background.[3]

Up to five photoreceptor GCs have been identified in the vertebrate retina, presumably generated by multiple gene duplications (42). Mammalian GC1 and GC2 have closely related photoreceptor guanylate cyclase orthologs in teleost (*Oryzias latipes*) and zebrafish (*Danio rerio*), but in mammalian retina only GC1 and GC2 have been identified. The absence of a photoreceptor response in the GCdko retina provides evidence that the mouse retina does not contain another GC, soluble or particulate, that can sustain phototransduction. A surprising consequence of GC deletion in mice was that several membrane-associated phototransduction proteins were down-regulated. The down-regulation of GCAPs and PDE6 (Figs. 5 and 7) and cone transducin (Figs. 6 and 7) in double knock-out retinas is considered posttranslational, because *Guca1a*, *Guca1b*, *Pde6a*, and *Pde6c* mRNA concentrations in WT and GCdko are unchanged, as evidenced by semiquantitative real time RT-PCR (Fig. 7*B*) and microarray analysis (not shown). Posttranslational down-regulation of these proteins may result from several mechanisms, including proteolytic degradation, protein instability, and impeded vesicular transport. GCAPs have been shown to be susceptible to proteolysis in low free Ca^{2+} *in vitro* (43) conditions presumed to be predominant in the GCdko and $GC1^{-/-}$ photoreceptors in which cation channels are closed. Therefore, proteolytic degradation of GCAPs in low [Ca^{2+}] could provide a mechanism for GCAP down-regulation. However, transducin (44) and PDE6 subunits (45) can be expressed stably in tissue culture in the absence of GC, cGMP, or external Ca^{2+}. It seems unlikely that low occupation of non-catalytic cGMP binding sites (GAF domains) (46) present on catalytic subunits influences PDE6 stability.

Common to all down-regulated proteins is their membrane association, either directly via prenyl or acyl anchors or indirectly by interaction with integral membrane proteins (GCAPs with GCs). Peripheral membrane-associated proteins are firmly bound to the membrane surface, are nondiffusible, and therefore must be transported to the site of ROS membrane assembly. Mechanistic details of transport of membrane-associated proteins are unknown. A vesicular transport pathway for rhodopsin from the endoplasmic reticulum to the outer segments has been firmly established (47-50). Transmembrane GCs probably follow a similar pathway. Outer segments of mouse photoreceptors undergo renewal about every 10 days

[3] $GC1^{-/-}$ mice used in this work were rederived on a C57BL6 background (19); $GC1^{-/-}$ used by Garbers and co-workers (18) were on a mixed 129SV/C57BL6 background.

(51), a high turnover rate requiring active biosynthesis and efficient transport. Thus, transport and targeting of membrane proteins to the outer segments is a pathway that is essential for function and survival of photoreceptors. We surmise that peripheral membrane proteins may attach to vesicular transport carriers for transport to the outer segments.

Knock-out of GCs does not affect the rhodopsin transport pathway, because rhodopsin is found at nearly normal levels in GCdko ROS (Fig. 7*A*, S1*D*). Therefore, GC transport and rhodopsin transport in rods must occur independently. Deletion of one GC does not affect stability and/or transport of PDE6 subunits in rods, but deletion of both GCs leads to PDE6 removal as evidenced by the absence of PDE6 signal on immunoblots (Fig. 7*A*). The presence of at least one GC is essential for PDE6 survival.

Knock-out of GC1, the only GC present in cones, strongly affects levels of S-cone and M/L-cone pigments (Figs. 6*B* and S2*B*). Both pigments localized to membranes that appear in part detached from the cone inner segments in GC1 and GCdko mutants. A second distinction between rods and cones is that acylated cone Tα and farnesylated cone Tγ were undetected in GC1$^{-/-}$ COS (Fig. 6, *F* and *J*), whereas acylated rod Tα (Fig. S1*H*) and farnesylated rod Tγ (results not shown) distributed normally in GC1$^{-/-}$ and GCdko rods. Third, GRK1 was undetectable in GC1$^{-/-}$ and GCdko COS but present in ROS. Thus, GC deletions affect rod and cone photoreceptor outer segments differently, suggesting that separate pathways have evolved in rods and cones for transport of membrane proteins. GC1 deletion only affects cones, whereas GC2 deletion has no effect on distribution of membrane-associated proteins. Deletion of both GCs has the additional effect of preventing PDE6 transport to the ROS.

It is noteworthy that in the absence of GCs, rod and cone outer segment membranes are assembled unconventionally, become unstable, and eventually disintegrate. Electron microscopy of GC knock-outs (Fig. 8) reveals an apparent “partitioning” of membrane components such that GCdko rod outer segments are composed of alternating bands of dense membrane stacks and lumen-containing tubules within a plasma membrane, whereas GC1$^{-/-}$ cone outer segments are composed of irregular collections of vesicle/tubules segregated from dense membrane layers. Conceivably, as transmembrane proteins, the presence of GCs may provide a structural scaffold that supports stabilization of disk morphogenesis by integrating membrane components. Further, the GC deletion phenotype is predicted to have low levels of cytoplasmic cGMP, resulting in permanently closed CNG cation channels and low $[Ca^{2+}]_i$, a situation mimicking constant light without phototransduction signaling. Mutations mimicking constant light (“equivalent light hypothesis”) have been proposed to trigger retinal degenerations in several, diverse animal models (52).

The GCdko retina degeneration phenotype is characterized by low levels of cGMP and is accompanied by a rod PDE6 knockdown. This suggests that the recessive retinal degeneration in the *rd1* mouse (53,54), which has high levels of cGMP due to an incapacitated PDE6, cannot be rescued by deletion of GCs.

In summary, our genetic, biochemical, and physiological approach to elucidate the function of GCs in mouse rod and cone photoreceptors revealed that GC1 and GC2 are the only cyclases involved in phototransduction. We have found no evidence for a role of soluble GCs or a third particulate GC as is known to exist in fish (55). GC1 appears to be a dominant enzyme, particularly in cones, but GC2 can effectively produce cGMP in the absence of GC1 in rods. Deletion of both GCs results in an animal model without rod and cone vision and a phenotype of a recessive cone/rod dystrophy resembling human Leber congenital amaurosis.

Acknowledgements

We are indebted to Dr. Sue Semple-Rowland (University of Florida) for providing GC1$^{-/-}$ mice and for numerous constructive comments on the manuscript.

References

1. Lowe DG, Dizhoor AM, Liu K, Gu Q, Spencer M, Laura R, Lu L, Hurley JB. Proc Natl Acad Sci USA 1995;92:5535–5539. [PubMed: 7777544]
2. Garbers DL, Lowe DG. J Biol Chem 1994;269:30741–30744. [PubMed: 7982997]
3. Yang RB, Garbers DL. J Biol Chem 1997;272:13738–13742. [PubMed: 9153227]
4. Duda T, Koch KW. Mol Cell Biochem 2002;230:107–116. [PubMed: 11952085]
5. Seebacher T, Beitz E, Kumagami H, Wild K, Ruppersberg JP, Schultz JE. Hear Res 1999;127:95–102. [PubMed: 9925020]
6. Palczewski K, Polans AS, Baehr W, Ames JB. Biol Essays 2000;22:337–350.
7. Dizhoor AM, Hurley JB. Methods 1999;19:521–531. [PubMed: 10581151]
8. Koch KW. Adv Exp Med Biol 2002;514:349–360. [PubMed: 12596932]
9. Lamb TD, Pugh EN Jr. Investig Ophthalmol Vis Sci 2006;47:5138–5152.
10. Burns ME, Mendez A, Chen J, Baylor DA. Neuron 2002;36:81–91. [PubMed: 12367508]
11. Haeseleer F, Sokal I, Li N, Pettenati M, Rao N, Bronson D, Wechter R, Baehr W, Palczewski K. J Biol Chem 1999;274:6526–6535. [PubMed: 10037746]
12. Mendez A, Burns ME, Sokal I, Dizhoor AM, Baehr W, Palczewski K, Baylor DA, Chen J. Proc Natl Acad Sci USA 2001;98:9948–9953. [PubMed: 11493703]
13. Noll GN, Billek M, Pietruck C, Schmidt KF. Neuropharmacology 1994;33:1407–1412. [PubMed: 7532822]
14. Cao L, Blute TA, Eldred WD. Vis Neurosci 2000;17:319–329. [PubMed: 10910101]
15. Tucker CL, Ramamurthy V, Pina AL, Loyer M, Dharmaraj S, Li Y, Maumenee IH, Hurley JB, Koenekoop RK. Mol Vis 2004;10:297–303. [PubMed: 15123990]
16. Hanein S, Perrault I, Gerber S, Tanguy G, Barbet F, Ducroq D, Calvas P, Dollfus H, Hamel C, Lopponen T, Munier F, Santos L, Shalev S, Zafeiriou D, Dufier JL, Munnich A, Rozet JM, Kaplan J. Hum Mutat 2004;23:306–317. [PubMed: 15024725]
17. Semple-Rowland SL, Lee NR, Van Hooser JP, Palczewski K, Baehr W. Proc Natl Acad Sci USA 1998;95:1271–1276. [PubMed: 9448321]
18. Yang RB, Robinson SW, Xiong WH, Yau KW, Birch DG, Garbers DL. J Neurosci 1999;19:5889–5897. [PubMed: 10407028]
19. Coleman JE, Zhang Y, Brown GA, Semple-Rowland SL. Investig Ophthalmol Vis Sci 2004;45:3397–3403. [PubMed: 15452041]
20. Rozet JM, Perrault I, Gerber S, Hanein S, Barbet F, Ducroq D, Souied E, Munnich A, Kaplan J. Investig Ophthalmol Vis Sci 2001;42:1190–1192. [PubMed: 11328726]
21. Bhosale P, Larson AJ, Frederick JM, Southwick K, Thulin CD, Bernstein PS. J Biol Chem 2004;279:49447–49454. [PubMed: 15355982]
22. Haire SE, Pang J, Boye SL, Sokal I, Craft CM, Palczewski K, Hauswirth WW, Semple-Rowland SL. Investig Ophthalmol Vis Sci 2006;47:3745–3753. [PubMed: 16936082]
23. Pennesi ME, Howes KA, Baehr W, Wu SM. Proc Natl Acad Sci USA 2003;100:6783–6788. [PubMed: 12732716]
24. Otto-Bruc A, Fariss RN, Haeseleer F, Huang J, Buczylko J, Surgucheva I, Baehr W, Milam AH, Palczewski K. Proc Natl Acad Sci USA 1997;94:4727–4732. [PubMed: 9114059]
25. Zhao X, Huang J, Khani SC, Palczewski K. J Biol Chem 1998;273:5124–5131. [PubMed: 9478965]
26. Howes KA, Bronson JD, Dang YL, Li N, Zhang K, Ruiz CC, Helekar BS, Lee M, Subbaraya I, Kolb H, Chen J, Baehr W. Investig Ophthalmol Vis Sci 1998;39:867–875. [PubMed: 9579466]
27. Haeseleer F, Imanishi Y, Maeda T, Possin DE, Maeda A, Lee A, Rieke F, Palczewski K. Nat Neurosci 2004;7:1079–1087. [PubMed: 15452577]

28. Maeda A, Maeda T, Imanishi Y, Kuksa V, Alekseev A, Bronson JD, Zhang H, Zhu L, Sun W, Saperstein DA, Rieke F, Baehr W, Palczewski K. J Biol Chem 2005;280:18822–18832. [PubMed: 15755727]
29. Van Hooser JP, Aleman TS, He YG, Cideciyan AV, Kuksa V, Pittler SJ, Stone EM, Jacobson SG, Palczewski K. Proc Natl Acad Sci USA 2000;97:8623–8628. [PubMed: 10869443]
30. Liang Y, Fotiadis D, Maeda T, Maeda A, Modzelewska A, Filipek S, Saperstein DA, Engel A, Palczewski K. J Biol Chem 2004;279:48189–48196. [PubMed: 15337746]
31. Kim TS, Maeda A, Maeda T, Heinlein C, Kedishvili N, Palczewski K, Nelson PS. J Biol Chem 2005;280:8694–8704. [PubMed: 15634683]
32. Luo DG, Yau KW. J Gen Physiol 2005;126:263–269. [PubMed: 16129773]
33. Frederick JM, Krasnoperova NV, Hoffmann K, Church-Kopish J, Ruether K, Howes KA, Lem J, Baehr W. Investig Ophthalmol Vis Sci 2001;42:826–833. [PubMed: 11222546]
34. Yang RB, Fulle HJ, Garbers DL. Genomics 1996;31:367–372. [PubMed: 8838319]
35. Howes KA, Pennesi ME, Sokal I, Church-Kopish J, Schmidt B, Margolis P, Frederick JM, Rieke F, Palczewski K, Wu SM, Detwiler PB, Baehr W. EMBO J 2002;21:1545–1554. [PubMed: 11927539]
36. Pepperberg DR, Birch DG, Hood DC. Vis Neurosci 1997;14:73–82. [PubMed: 9057270]
37. Lyubarsky AL, Pugh EN Jr. J Neurosci 1996;16:563–571. [PubMed: 8551340]
38. Coleman JE, Semple-Rowland SL. Investig Ophthalmol Vis Sci 2005;46:12–16. [PubMed: 15623748]
39. Milam AH, Barakat MR, Gupta N, Rose L, Aleman TS, Pianta MJ, Cideciyan AV, Sheffield VC, Stone EM, Jacobson SG. Ophthalmology 2003;110:549–558. [PubMed: 12623820]
40. Chen CK, Burns ME, Spencer M, Niemi GA, Chen J, Hurley JB, Baylor DA, Simon MI. Proc Natl Acad Sci USA 1999;96:3718–3722. [PubMed: 10097103]
41. Lyubarski AL, Chen C-K, Simon MI, Pugh EN Jr. J Neurosci 2000;20:2209–2217. [PubMed: 10704496]
42. Imanishi Y, Yang L, Sokal I, Filipek S, Palczewski K, Baehr W. J Mol Evol 2004;59:204–217. [PubMed: 15486694]
43. Rudnicka-Nawrot M, Surgucheva I, Hulmes JD, Haeseleer F, Sokal I, Crabb JW, Baehr W, Palczewski K. Biochemistry 1998;37:248–257. [PubMed: 9425045]
44. Min KC, Gravina SA, Sakmar TP. Protein Expression Purif 2000;20:514–526.
45. Qin N, Baehr W. J Biol Chem 1994;269:3265–3271. [PubMed: 8106363]
46. Mou H, Cote RH. J Biol Chem 2001;276:27527–27534. [PubMed: 11375400]
47. Deretic D, Williams AH, Ransom N, Morel V, Hargrave PA, Arendt A. Proc Natl Acad Sci USA 2005;102:3301–3306. [PubMed: 15728366]
48. Deretic D. Eye 1998;12:526–530. [PubMed: 9775213]
49. Sung CH, Tai AW. Int Rev Cytol 2000;195:215–267. [PubMed: 10603577]
50. Tai AW, Chuang JZ, Bode C, Wolfrum U, Sung CH. Cell 1999;97:877–887. [PubMed: 10399916]
51. Besharse JC, Hollyfield JG. Invest Ophthalmol Vis Sci 1979;18:1019–1024. [PubMed: 478775]
52. Lem J, Fain GL. Trends Mol Med 2004;10:150–157. [PubMed: 15059605]
53. Pittler SJ, Baehr W. Proc Natl Acad Sci USA 1991;88:8322–8326. [PubMed: 1656438]
54. Bowes C, Li T, Danciger M, Baxter LC, Applebury ML, Farber DB. Nature 1990;347:677–680. [PubMed: 1977087]
55. Hisatomi O, Honkawa H, Imanishi Y, Satoh T, Tokunaga F. Biochem Biophys Res Commun 1999;255:216–220. [PubMed: 10049688]

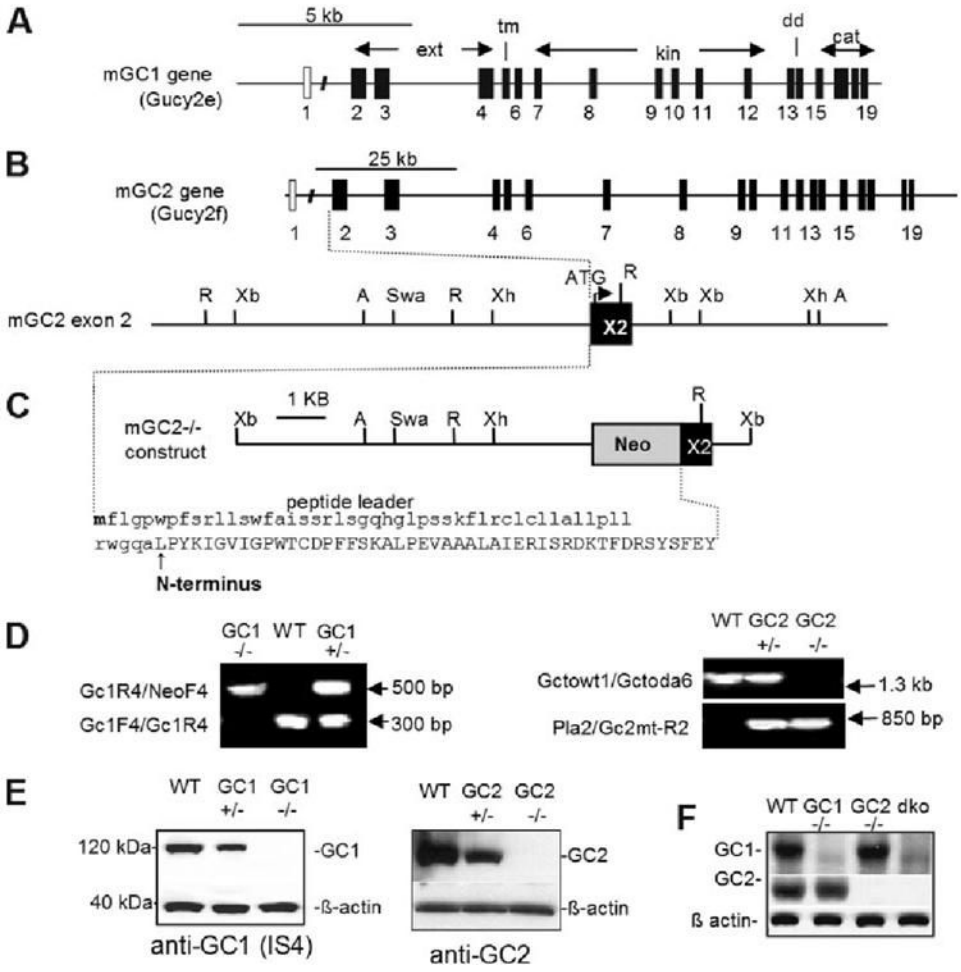

FIGURE 1. Mouse GC1 and GC2 gene structures, knock-out constructs, genotyping, and controls

The mouse GC1 (*Gucy2e*) (*A*) and the mouse GC2 (*Gucy2f*) (*B*) genes each consist of 19 exons (*black boxes*). Exons 2–4 encode the extracellular domain (*ext*), exon 5 encodes the transmembrane domain (*tm*), exons 6–12 encode the kinase homology domain (*kin*), exons 13 and 14 encode the dimerization or hinge domain (*dd*), and exons 15–19 encode the catalytic domain (*cat*). The knock-out construct of the mGC1 gene deletes 17 of 24 transmembrane residues (18). *C*, the knock-out construct of the mGC2 gene deletes a portion of exon 2 that includes ATG, the peptide leader sequence, and a portion of the mature N terminus of mGC2. *D*, PCR genotyping WT and knock-out GC1 gene (*left*) and genotyping the WT and knock-out GC2 gene (*right*). Diagnostic fragments for WT Gc1 (Gc1F4/G11R4) and knock-out Gc1 (NeoF4/Gc1R4) are 290 and 575 bp in size, respectively. Diagnostic fragments for WT GC2 (Gctowt1/Gctoda6) and knock-out GC2 (Pla2/Gc2mt-R2) are 1395 and 852 bp in size, respectively. *E*, immunoblots of retinal lysates probed with a polyclonal anti-GC1 antibody (*left*) and with a polyclonal anti-GC2 antibody (*right*). *F*, immunoblots of retinal lysates probed with polyclonal anti-GC1 and -GC2 antibodies. Anti-*β*-actin antibody was used as an internal control for loading.

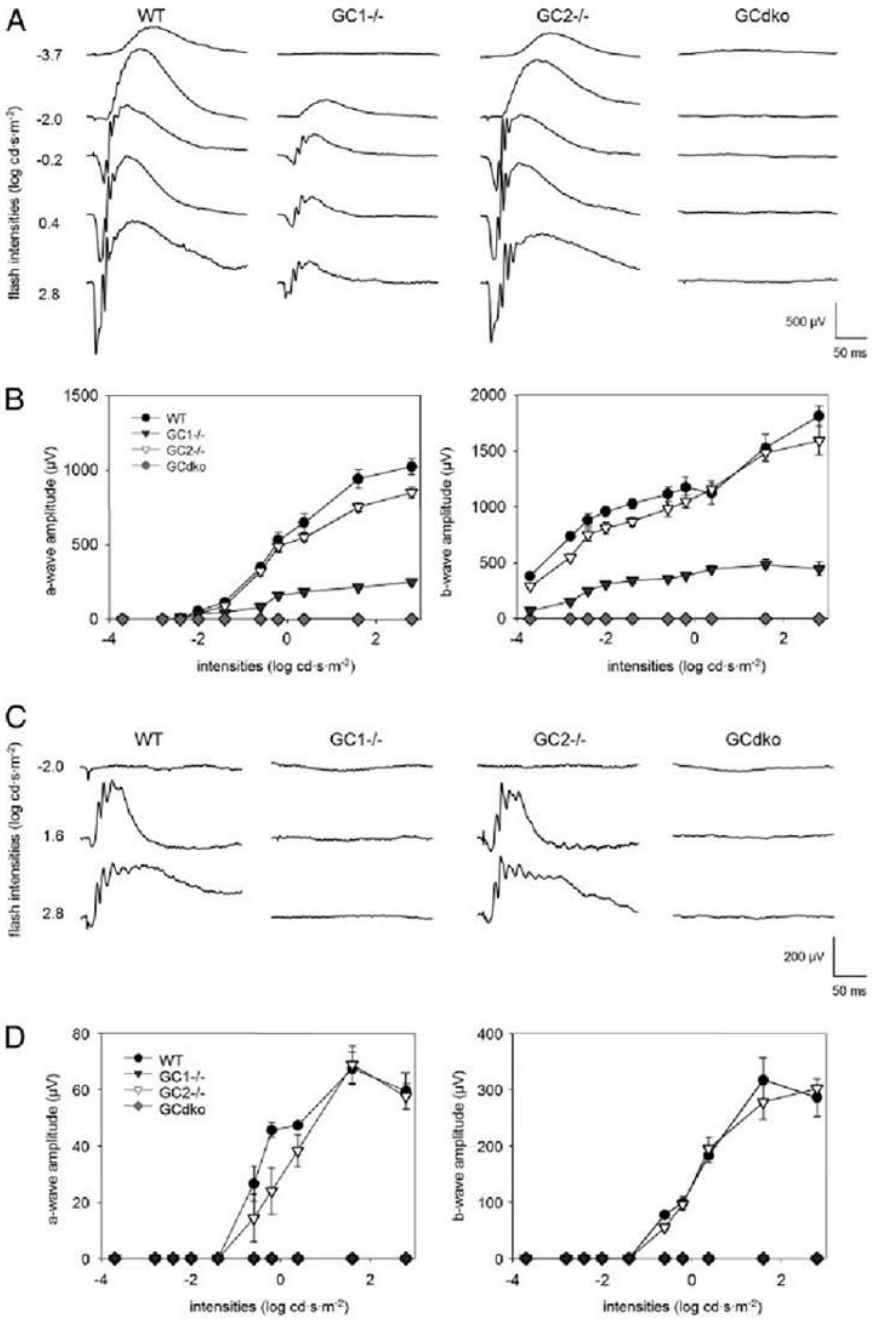

FIGURE 2. Full field ERGs of WT and GC deletion mutant mice under scotopic and photopic conditions

A, serial responses to increasing intensities of flash stimuli were obtained from dark-adapted WT, GC1$^{-/-}$, GC2$^{-/-}$, and GCdko mice. Although the GC1$^{-/-}$ response was severely attenuated, only double knock-out mice failed to produce any ERG responses. *B*, the a- and b-wave amplitudes, respectively, plotted as a function of light intensity under dark-adapted conditions. *C*, three representative serial responses to increasing intensities of flash stimuli were obtained from light-adapted WT, GC1$^{-/-}$, GC2$^{-/-}$, and GCdko mice. *D*, a- and b-wave amplitudes plotted as a function of light intensity under light-adapted conditions. 4 – 6 littermates of each genotype were used for analysis.

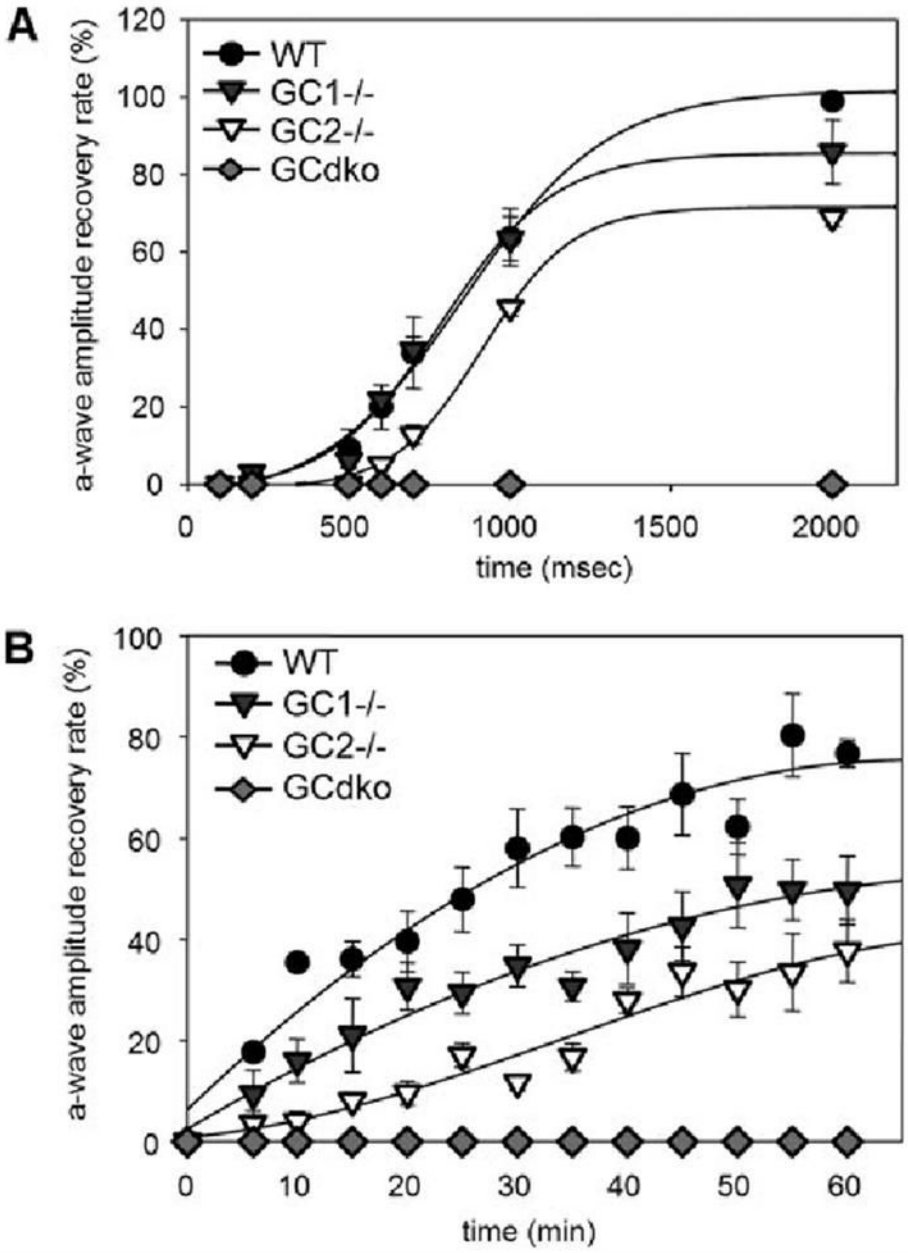

FIGURE 3. Measurements of a-wave recovery after a conditioning flash and after constant light stimulation

A, normalized recovery of a-wave amplitude as a function of interstimulus interval between the test and probe flashes. The dark-adapted mice were conditioned first with the test flash (0.4 log·cd·s·m^{-2}) followed by a probe flash (1.6 log·cd·s·m^{-2}) with interstimulus intervals ranging from 200 to 2,000 ms. Each *trace* represents the average recording from eight eyes. The interstimulus interval required to reach 50% a-wave amplitude recovery was not significantly different among genetic backgrounds (Table 1). As expected, GCdko photoreceptors were unresponsive. *B*, measurements of a-wave recovery following constant light stimulation. Dark-adapted mice were bleached with intense constant illumination (500 cd·s·m^{-2}) for 3 min, and recovery of a-wave amplitude was monitored by recording single-flash ERGs (−0.2 log·cd·s·m^{-2}) over the course of a 60-min dark adaptation period; the recovery ratio is plotted.

The ratio in $GC1^{-/-}$, $GC2^{-/-}$, and GCdko mice was significantly attenuated compared with WT ($GC1^{-/-}$ and $GC2^{-/-}$ compared with WT, $p < 0.001$; GCdko compared with WT, $p < 0.0001$), and the ratio in GC2−/− was significantly attenuated relative to $GC1^{-/-}$ mice ($GC1^{-/-}$ to $GC2^{-/-}$, $p < 0.05$).

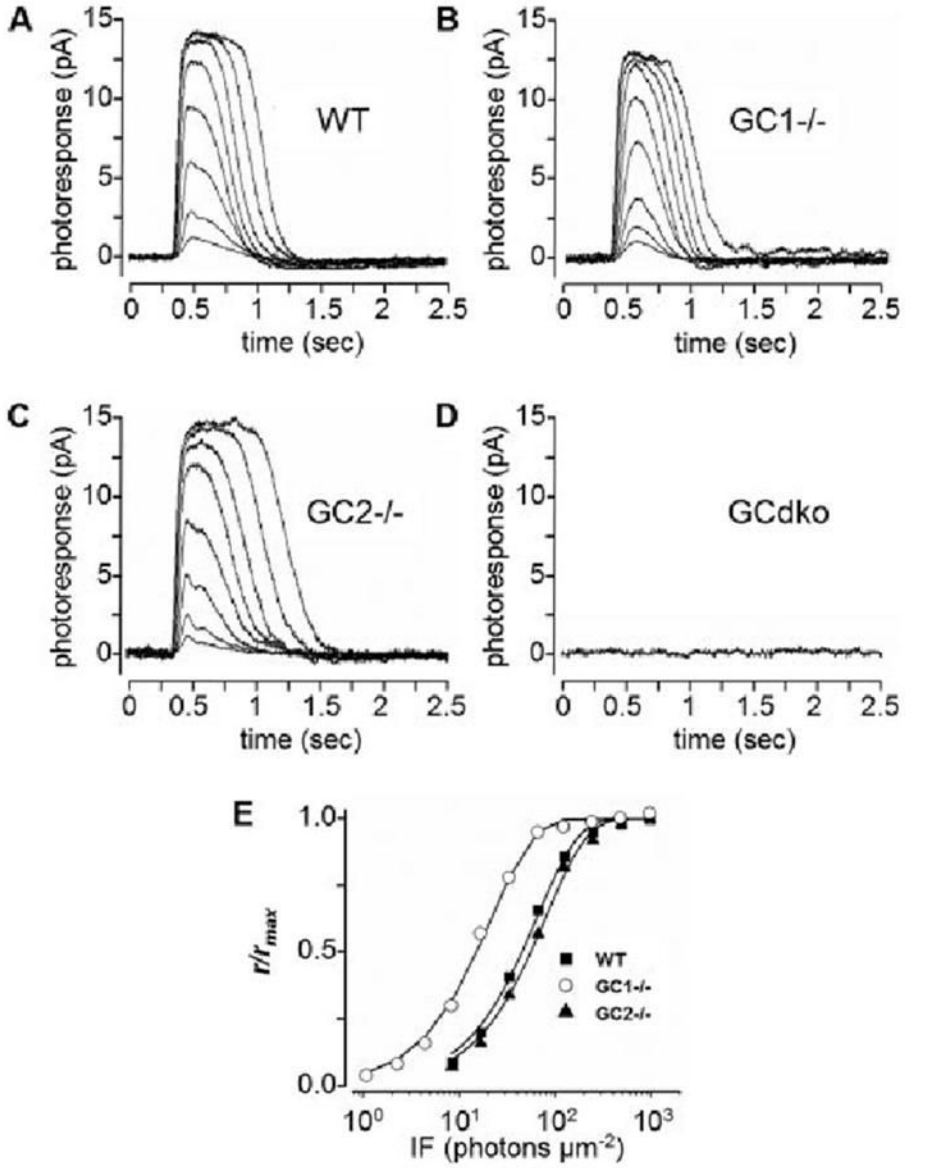

FIGURE 4. Suction pipette recordings from single rods of WT and GC1/2 knock-out mice

A–D, flash response families measured for a WT rod (*A*), a GC1$^{-/-}$ rod (*B*), a GC2$^{-/-}$ rod (*C*), and a GCdko rod (*D*). Each *panel* superimposes average responses to 10 – 60 flash stimuli with the flash strength increasing by a factor of 2 in *A–C*. The flash strengths were 8.4, 16.7, 33.3, 66.5, 123.4, 246.7, 485.1, and 970.2 photons μm^{-2} for both *A* and *C*; 2.3, 4.5, 8.4, 16.7, 33.3, 66.5, 123.4, 246.7 and 485.1 photons μm^{-2} for *B*; and 970.2 photons μm^{-2} for *D*. *E*, stimulus-response relationships for the cells shown in *A–C*. Peak response amplitudes normalized to saturating response amplitude are plotted against the flash strength. Data were fitted with saturating exponential functions that were used to estimate the strength of the flash producing a half-maximal response (WT, 45 photons μm^{-2}; GC1$^{-/-}$, 15 photons μm^{-2}; GC2$^{-/-}$, 55 photons μm^{-2}). A flash of 500 nm with a duration of 10 ms was delivered at 300 ms.

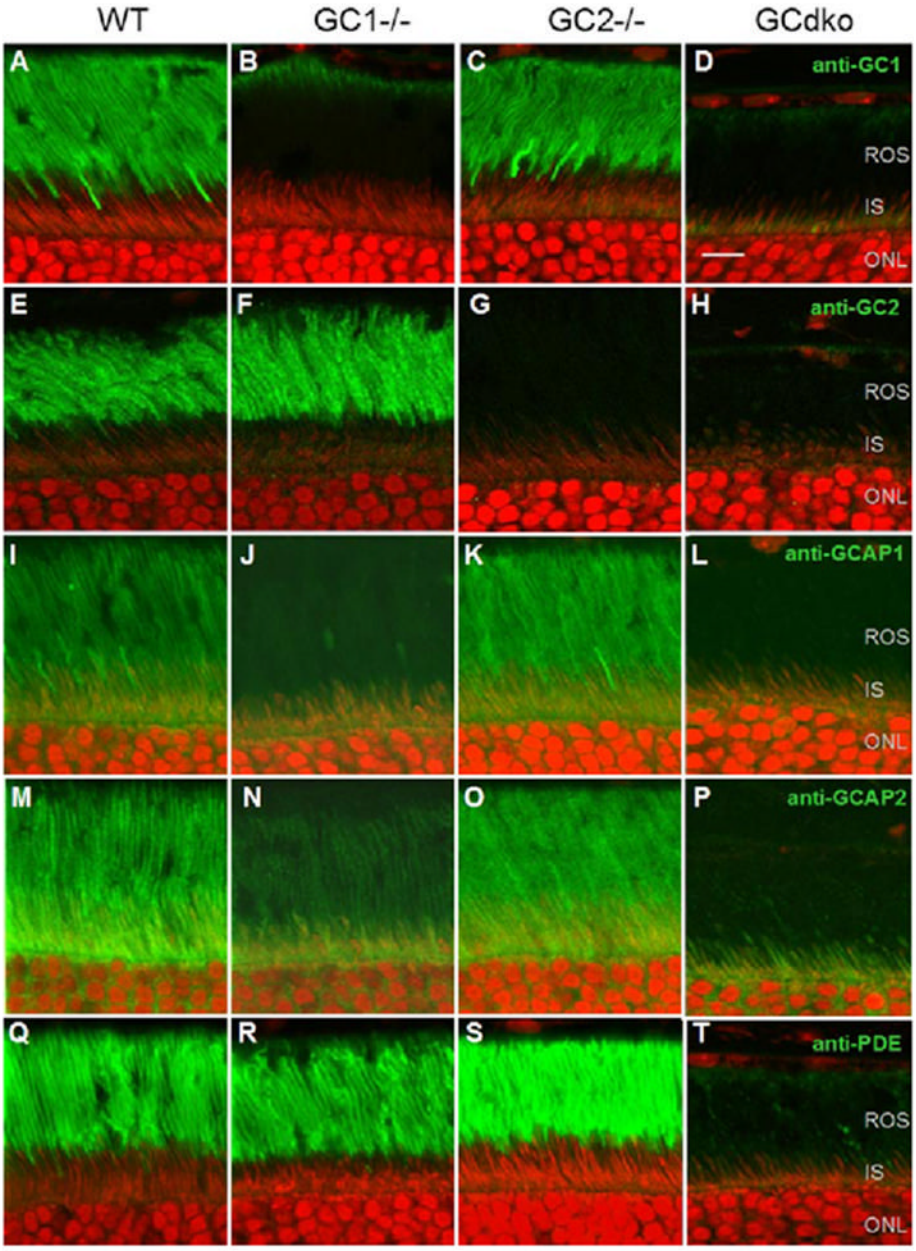

FIGURE 5. Confocal immunolocalization of GC1, GC2, GCAP1, GCAP2, and rod PDE6 in photoreceptors of WT and GC deletion mutant mice, aged 1–2 months

A–D, localization of GC1 (mAb IS4); *E–H*, localization of GC2 (pAb L670) in WT, $GC1^{-/-}$, $GC2^{-/-}$, and GCdko retina sections, respectively. GC1 (*green*) is absent in photoreceptors of $GC1^{-/-}$ retina, and GC2 is absent in $GC2^{-/-}$ retina, and both are absent in GCdko retina. Localizations of GCAP1 (pAb UW14) (*I–L*) and GCAP2 (pAb UW50) (*M–P*) are indicated by fluorescein isothio-cyanate-conjugated secondary antibody. Both GCAPs appear down-regulated in photoreceptors of $GC1^{-/-}$ and GCdko retina. *Q–T*, immunolocalization of rod PDE6 (*green*; MOE) in WT, $GC1^{-/-}$, $GC2^{-/-}$, and GCdko retina sections, respectively. Note that rod PDE6 is absent in GCdko retina. Sections were contrasted with propidium iodide to allow visualization of cell nuclei. *IS*, inner segments; *ONL*, outer nuclear layer. *Magnification bars*, 10 μm.

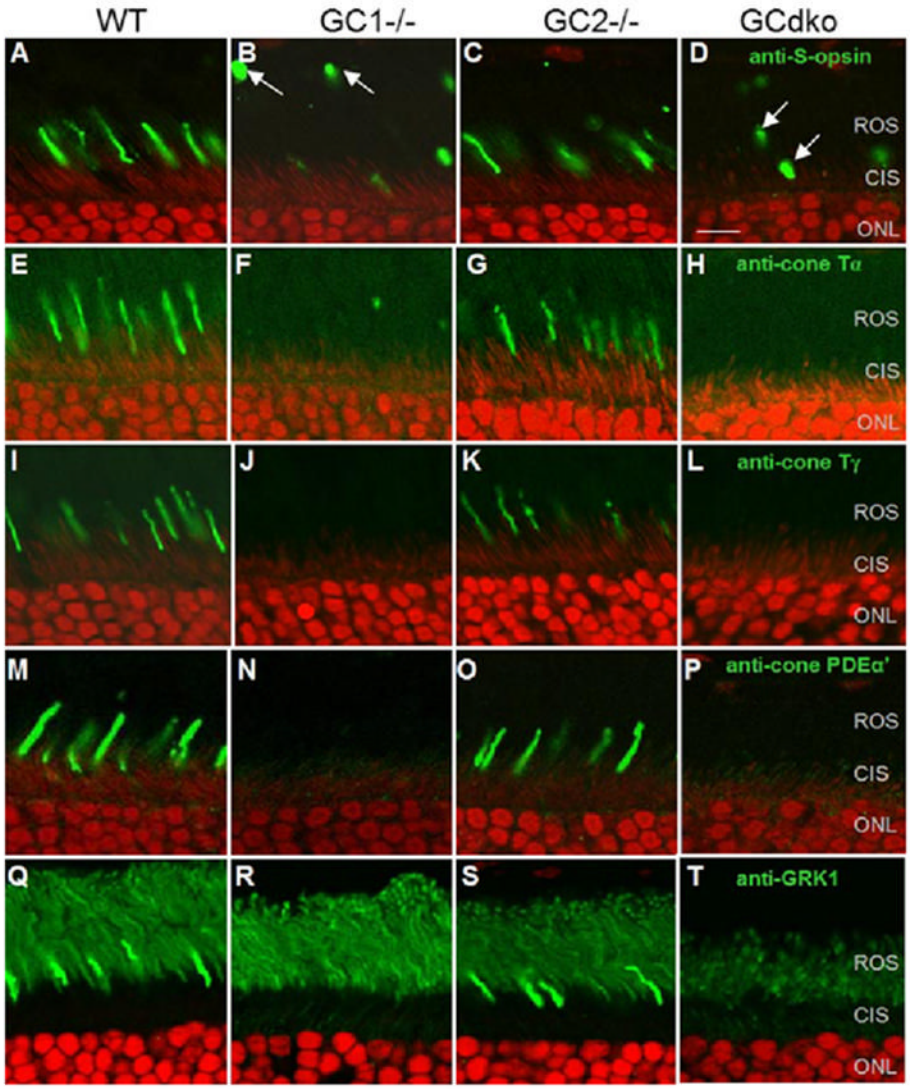

FIGURE 6. Immunolocalization of S-opsin, cone T*α*, cone T*γ*, cone PDE6*α′*, and GRK1 in retinas of WT and GC deletion mutants, aged 1–2 months

A–D, localization of S-opsin; *E–H*, cone T*α*; *I–L*, cone T*γ*, *M–P*, cone PDE6*α′* *Q–T*, GRK1 in WT, GC1$^{-/-}$, GC2$^{-/-}$, and GCdko retinas, respectively. S-opsin, cone T*α*, cone T*γ*, cone PDE6*α′*, and GRK1 were localized normally to WT and GC2$^{-/-}$ COS. S-opsin mislocalizes to COS fragments in GC1$^{-/-}$ and GCdko retinas. Cone T*α*, cone T*γ*, and cone PDE6*α′* appear down-regulated in GC1$^{-/-}$ and GCdko retinas. Anti-GRK1 labels cone outer segments prominently in the proximal OS layer, whereas the remainder is attributable to ROS. GRK1 is present in ROS of all four genotypes and in WT and GC2$^{-/-}$ COS but absent in GC1$^{-/-}$ and GCdko COS. *Magnification bars*, 10 μm.

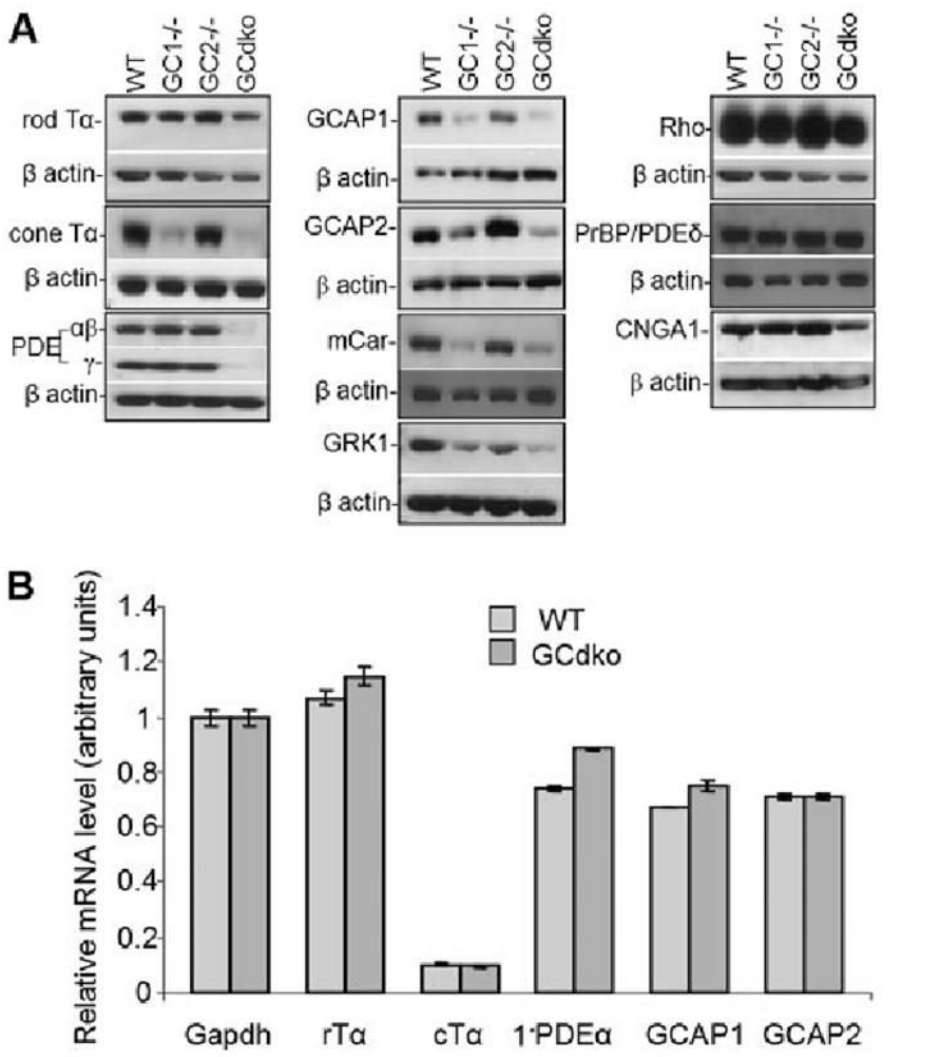

FIGURE 7. Immunoblots and transcript levels of down-regulated phototransduction components

A, immunoblots of WT, GC1$^{-/-}$, GC2$^{-/-}$, and GCdko retina lysates probed with anti-rod T*α*, anti-cone T*α*, anti-rod PDE6, anti-GCAP1, anti-GCAP2, anti-cone arrestin, and anti-GRK1 antibodies. Immunoblots of rhodopsin, PrBP/*δ*, and CNGA1, which are not down-regulated, are shown as controls. Internal controls with *β*-actin demonstrate loading levels. *B*, semiquantitative real time RT-PCR of different transcripts (rod T*α*, cone T*α*, rod PDE6*α*, GCAP1, and GCAP2). Duplicate samples were determined, each using two retinas of different animals, and run in parallel with Gapdh-specific primers as a standard. The relative mRNA expression level is defined as the fluorescence of each sample normalized to the fluorescence of Gapdh. Note that cone T*α* levels are lower, since less than 10% of photoreceptors are cones.

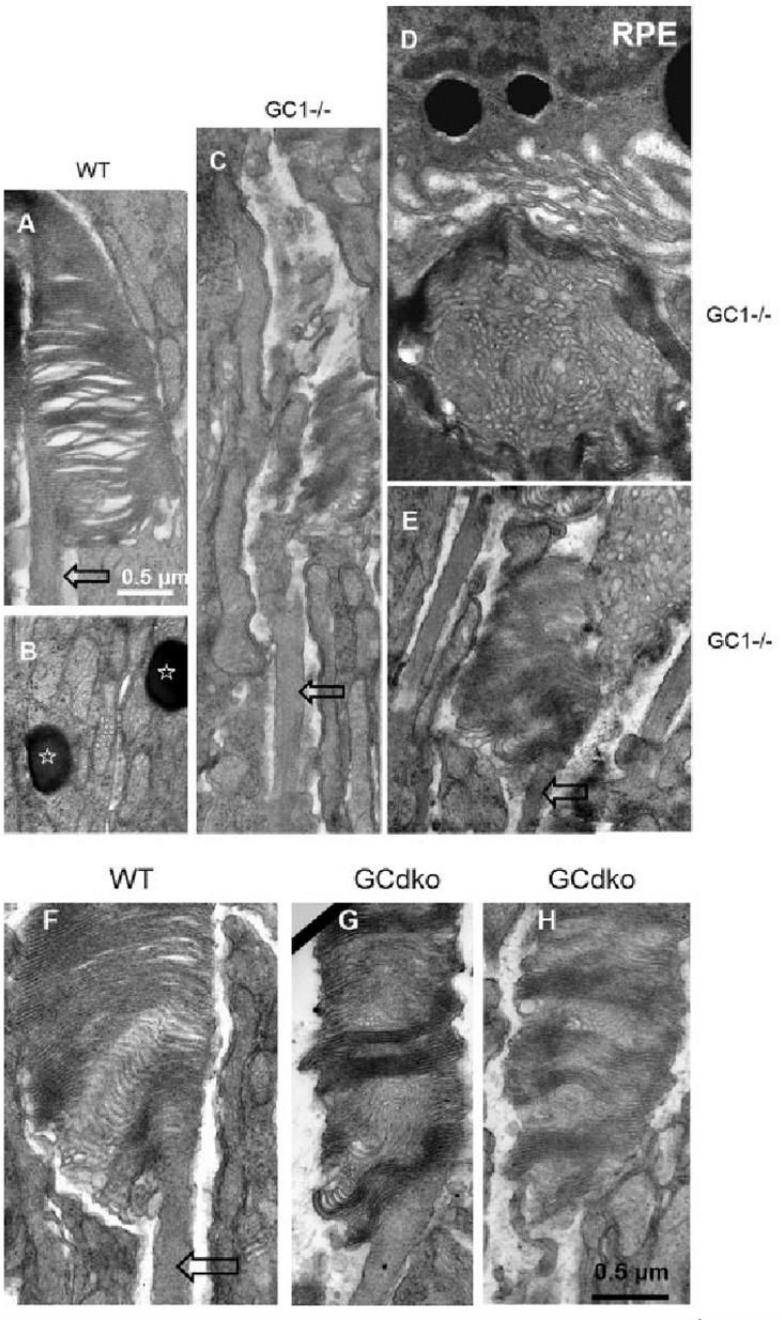

FIGURE 8. Ultrastructure of WT (*A* and *B*) and degenerative GC1$^{-/-}$ (*C–E*) cone outer segments

A, *open arrows* denote connecting cilia of cone photoreceptors for reference. The WT cone outer segment measures 1.3 μm at its widest point and tapers distally; *B*, cone inner segments were sometimes observed to contain electron-dense granules (*stars*). *C*, disorganized GC1$^{-/-}$ cone outer segment reveals apparent partitioning of membrane components; lamellar structures emanate from one side of the distal connecting cilium and vesicles from the tip. *D*, adjacent to the retinal pigmented epithelium (*RPE*), extracellular particle (2–3 μm in diameter) containing vesicles and tubules surrounded by membrane lamellae appears as an end product of membrane component sorting. Such a particle probably corresponds to the opsin-immunoreactive particles shown in Fig. 6*B* (see also Figs. S2*B* and S2*J*). *E*, another example of membrane partitioning

is shown in which membrane layers are found to one side of the distal connecting cilium and vesicles/tubules extend from its tip. Cones were examined in a location inferior to the optic nerve for each genotype. *F–H*, electron micrographs of rod outer segments from WT and GCdko mouse retinas. The *open arrow* indicates the connecting cilium of the WT rod (*F*). Predegenerate ROS of GCdko retinas (*G* and *H*) have a striated appearance of alternating lamellae and tubules that may underlie the patchy patterns of rhodopsin kinase immunoreactivity observed in Fig. 6*T* and rod Tα immunoreactivity in Fig. S1*H*.

TABLE 1

ERG data (a-wave amplitudes, sensitivity, and recovery) for WT, GC1$^{-/-}$, and GC2$^{-/-}$ mice

	WT	GC1$^{-/-}$	GC2$^{-/-}$
Maximum a-wave amplitude (μV)	964.6 ± 48.4	239.3 ± 50.5[a]	874.8 ± 23.9
Sensitivity (log scotopic-cd^{-1} m^2 s^{-3})	6.2 ± 0.3	6.4 ± 1.2	4.4 ± 0.4[b]
Time between flashes for 50% a-wave amplitude recovery (ms)	893.3 ± 47.8	895.4 ± 112.2	1,018.1 ± 63.1

[a] $p < 0.0001$.

[b] $p < 0.05$.